Chapter 5

Volatiles, mineral stabilities and their effect on the forces driving exhumation of subducted continental crust in the Sesia Zone (Western Alps)

MATTHIAS KONRAD-SCHMOLKE, MARK R. HANDY AND JOCHEN BABIST

Freie Universität Berlin, Department of Earth Sciences, Malteserstrasse 74-100 D-12249 Berlin

5.1 ABSTRACT

The Sesia Zone (SEZ) in the Western Alps is one of the largest known bodies of continentally derived rocks to have undergone subduction-related high pressure (HP) metamorphism. It comprises two basement nappes, one of which preserves fresh HP mineral assemblages and fabrics. P-T trajectories for these assemblages derived from thermobarometry and thermodynamic modelling of chemically zoned metamorphic minerals indicate near-isothermal decompression from 1.8 to 1.1 GPa at temperatures of 500-550°C. Modelling of water fractionation along the pro- and retrograde P-T trajectory shows that water saturation of the mineral assemblage during initial decompression can be achieved without external water supply. This initial exhumation probably occurred along the slab-mantle interface, prior to or during transpression accommodated by mylonitic shearing under retrograde eclogite- to blueschist- to greenschist facies conditions. The SEZ then underwent further exhumation to 0.8 GPa and cooling from 500 to 400°C in the footwall of a moderately dipping, top to-E normal fault active under greenschist-facies conditions. Calculations of density and shear strength based on our forward modelling and on experimental rheological data indicate that initial exhumation to the base of the crust was driven by buoyancy

forces. Subsequent extensional exhumation within the crust was driven by tectonically induced forces acting on the upper plate of the subduction system.

5.2 INTRODUCTION

The observation that continental crust can be subducted to depths in excess of 100 km (Chopin, 1984; Zhang and Liou, 1994; O´Brien et al., 2001), and then returned to the surface without equilibrating on the way up has remained an geodynamic enigma in search of a consensus solution for just over 30 years (e.g. Platt 1993 and references therein). The preservation of high-pressure (HP) and, in some cases even ultra-high pressure (UHP) minerals like coesite and diamond, has been attributed variously to very fast exhumation (e.g. Rubatto and Herrmann, 2001; Massonne and O´Brien, 2003), to sluggish reaction kinetics favoured by anhydrous conditions during exhumation (Mosenfelder et al., 2005), or to exhumation along a pressure-temperature path with few or no retrograde reactions (Oberhänsli et al., 2002). These scenarios have been proposed for tectonic settings ranging from obduction along oblique-convergent margins (Karig 1980), buoyant rise within orogens (England and Holland 1979), to extensional exhumation during orogenesis (e.g., Platt 1986, Dewey 1989). In recent years, this first generation of models has been superceded by scaled analogue experiments (Chemenda et al., 1995) and thermo-mechanical, numerical models (e.g. Bousquet et al., 1997; Burov et al., 2001; Roselle and Engi, 2002; Gerya et al., 2002; Seyferth and Henk, 2004) which essentially demonstrate that HP and UHP rocks may be entrained within basement nappes that are either forcibly extruded (Jamieson et al., 2002) or undergo buoyant rise (Burov et al., 2001) within the upper plate of the convergent margin.

The Sesia Zone (SEZ) at the inner arc of the Western Alps (Fig. 5.1) is one of the first places where controversy over exhumation of HP rocks arose, primarily due to its early recognition as a coherent piece of continental crust that underwent eclogite-facies metamorphism in a subduction zone (Ernst, 1971; Compagnoni et al., 1977). Previously, the subduction of continental crust to depths of 60 km or more had been considered unlikely due to the positive buoyancy associated with the density contrast of continental crust and upper mantle rock. A plethora of petrological and geochronological studies initially supported the idea that the exhumation of Late Cretaceous HP rocks in the Sesia

Zone occurred in Mid- to Late Tertiary time (e.g., Oberhänsli et al. 1985) due to mylonitic backthrusting and erosion along the Insubric Line (Rubie 1984). The Insubric Line (Fig. 5.1) is a late orogenic fault that delimits the retro-wedge of the Tertiary Alpine orogen from the Southern Alps. However, this model was found to be incompatible with evidence that eclogites in the SEZ were exhumed already prior to Oligocene magmatism (e.g., Biella, Traversella plutons in Fig. 5.1) and Oligo-Miocene Insubric faulting (Fig. 5.1).

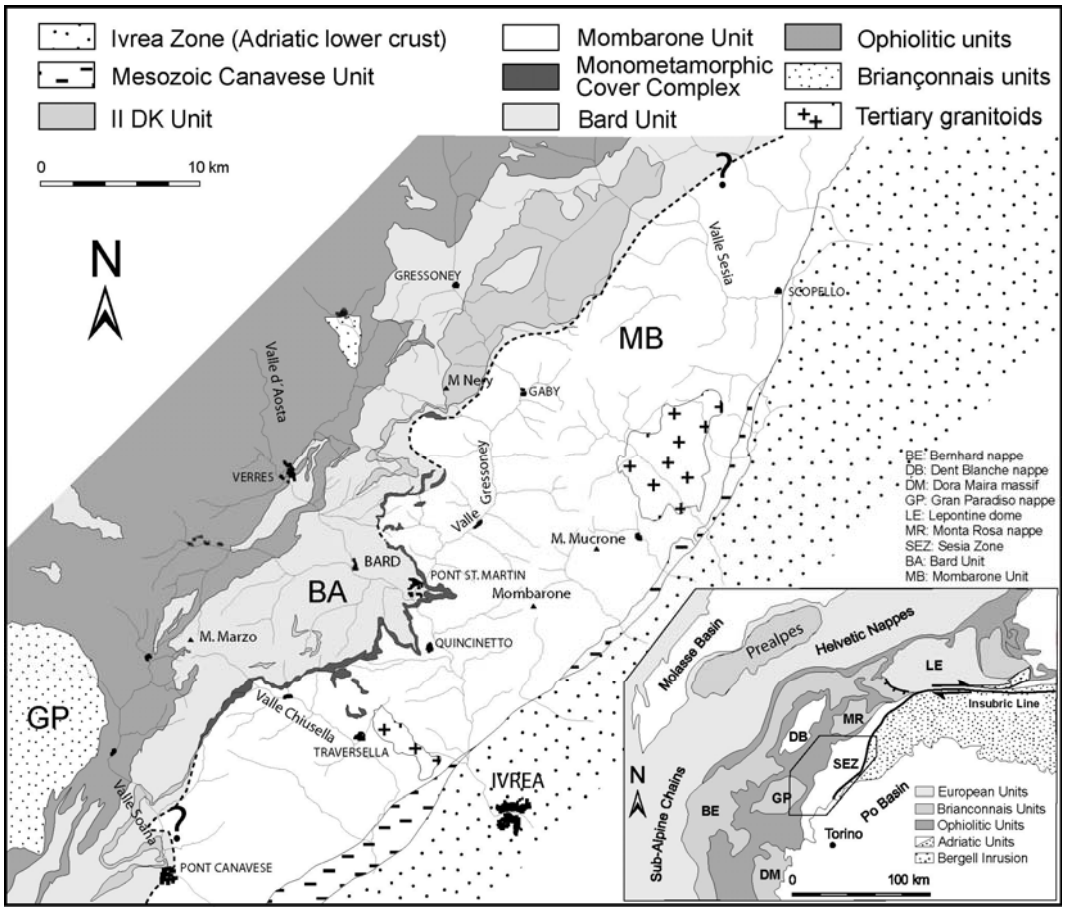

Fig. 5.1: Geological map of the central Sesia Zone. Mark the complex folding of the II DK and MCC rocks with the Bard and Mombarone Units.

Underlying the ongoing debate on the exhumation of coherent bodies of subducted continental crust is incomplete knowledge of the pressure-temperature path experienced by the rocks in these bodies. Moreover, direct structural evidence for the exhumation mechanism(s) is often scant or lacking due to deformational and metamorphic overprinting. Relics of the initial stages of exhumation are particularly susceptible to overprinting. The exhumation mechanisms can only be determined if pressure-temperature (P-T) paths for the exhumed crust can be correlated with structural and geochronological

information, enabling the construction of pressure-temperature-deformation-time or P-T-d-t paths for subducted and exhumed rock units. P-T paths are diagnostic of the tectonothermal evolution of the crust because they are function of the temperature gradient between the subducted plate and the overriding plate, the heat capacity of the subducted rocks and the residence time of the slab within the hotter mantle and lower crustal rocks. Yet, previous studies have shown that P-T curves also reflect the chemical evolution and elemental transport properties of the exhuming rocks (e.g., Konrad-Schmolke et al., 2005). The chemical evolution, especially the volatile content of the rocks, governs the tectonics of burial and exhumation because it affects mineral stabilities and reaction kinetics (e.g. Rubie 1990). Mineral reactions change the physical properties of the subducted slab and therefore can affect the dynamics of subduction (e.g., Hacker et al. 2003, Konrad-Schmolke et al., Chapter 3). To the extent that they are preserved, structures formed during the retrograde evolution yield complimentary insight into the dynamics of flow in the crust and mantle, and are key to unravelling the kinematics of exhumation.

The Sesia Zone preserves structures related to a complex sequence of deformational and metamorphic events experienced by its HP rocks during exhumation. The description of these structures in section 2 provides a context for the interpretation and modelling of growth features of HP minerals and parageneses in section 3. In particular, we apply forward thermodynamic modelling of local disequilibrium features like chemically zoned grains of HP minerals to derive synthetic P-T paths for the exhumation of the Sesia HP rocks. The validity of these paths is then assessed by comparing them with paths derived from conventional thermobarometry in well-equilibrated HP rocks. Chemical zonation patterns in minerals have been used before to constrain the P-T paths of their host rocks (e.g. Spear and Selverstone, 1983; Menard and Spear, 1993; Okudaira, 1996) and to determine element mobility and volatile content in metamorphic rocks (e.g. Carlson, 1989; Konrad-Schmolke et al., 2005). In section 3, we extend this approach to investigate the effects of fractional crystallisation and water fractionation in HP assemblages during exhumation of the Sesia Zone. Forward thermodynamic modelling yields insight into the physico-chemical processes during exhumation because the calculated mineral assemblages and the

mineral compositions are path-dependent and can be compared with the observed assemblages and compositions (Konrad-Schmolke et al., 2005).

Finally, in section 4 we extract information from the forward thermodynamic models on the density, water content and volumes of the pertinent phases in the HP rocks of the Sesia Zone. This allows us to estimate the buoyancy forces acting on the Sesia slab (Bousquet et al., 1997) during successive stages of exhumation through the lithosphere. Buoyancy of HP rocks as a possible driving force of their exhumation has been invoked almost since high-pressure metamorphism was recognized in continentally derived rocks (e.g. Ernst, 1971; England and Holland, 1979; Platt, 1993; Ernst, 2001; Carswell et al., 2003; Walsh and Hacker, 2004). We extrapolate experimental creep laws for a variety of minerals and deformation mechanisms to natural conditions in order to assess the relative magnitude of shear stresses related to buoyancy and to viscous creep at the boundaries of exhuming HP rock bodies. Our results show that although buoyancy was important during exhumation of the Sesia Zone within the mantle and lower continental crust, additional syn-orogenic, tectonic forces acted to exhume HP rocks within the intermediate and upper crust to the surface.

5.3 GEOLOGICAL SETTING

The Sesia Zone underwent HP metamorphism in Late Cretaceous time (Dal Piaz et al., 1972) during the initial stages of Cretaceous to Tertiary subduction of the European plate beneath the Apulian plate (Handy and Oberhänsli 2004 and references therein). Together with the Dent Blanche nappe and several Austroalpine outliers (Fig. 5.1), the SEZ forms the structurally highest unit of the Western Alpine nappe pile (e.g. Gosso, 1977; Gosso et al., 1979). Prior to subduction, the Sesia Zone occupied the distal part of the Apulian passive continental margin (e.g. Carraro et al., 1970; Dal Piaz et al., 1972) that was separated from the European continental margin by the Early Jurassic Piemont-Liguria Ocean. In Late Cretaceous time, the distal part of the Apulian margin, including the basement rocks that now form the Sesia Zone, was subducted to depths of about 60 km beneath the Apulian plate (e.g. Handy and Oberhänsli 2004). Mica ages in the Sesia Zone indicate that it was exhumed and cooled to temperatures in the range of 300-500°C already in Late Cretaceous to Early Tertiary time. The Piemont-Liguria oceanic units that presently underlie the Sesia

Zone preserve Early Tertiary HP and UHP mineral assemblages (e.g. Reinecke, 1991). The contact of these rocks with the Sesia Zone is marked by a greenschist-facies shear zone, the Gressoney Shear Zone that accommodated top-SE extension in Early Tertiary time (e.g. Reddy et al. 1999). South and east of the SEZ lie pre-Alpine, lower crustal and upper mantle rocks of the Southern Alpine Ivrea Zone. These rocks are only locally overprinted by weak, sub-greenschist facies metamorphism (Zingg et al., 1990) and are separated from the Sesia Zone by greenschist-facies mylonites of the Insubric Line (Fig. 5.1).

5.3.1 Lithotectonic subunits

Like other continental HP terranes, the Sesia Zone consists of a variety of continentally derived metamorphic rocks (e.g. Dal Piaz et al., 1972; Compagnoni et al., 1977). They can be divided into four different lithotectonic units (Fig. 5.1, Babist et al., Chapter 4):

(1) the Mombarone unit in the southeastern part of the SEZ is an elongate body of about 90 x 30 km in areal extent that comprises coarse-grained garnet-zoisite-omphacite-sodic amphibole-phengite gneiss and schist, smaller lenses of sodic amphibole-bearing basic eclogite, omphacite-phengite-zoisite-bearing marble as well as subordinate quartzite (e.g. Compagnoni et al., 1977; Castelli 1991; Ferraris and Compagnoni, 2003). Although most mineral parageneses have experienced retrograde overprinting, eclogite-facies assemblages are well preserved in areas marked by stars in Figure 5.2 (Dal Piaz et al., 1972, Compagnoni et al., 1977; Zucali et al., 2002). Peak metamorphic conditions of these rocks were about 500 to 600°C at pressures between 1.5 and 2.0 GPa (Dal Piaz et al. 1972; Compagnoni and Maffeo 1973; Reinsch, 1979; Desmons and O´Neil, 1978; Compagnoni et al., 1977; Oberhänsli et al., 1985; Koons, 1986; Vuichard and Ballèvre 1988; Pognante 1989; Tropper et al, 1999; Zucali et al., 2002). These rocks are cut by two Oligocene, granodioritic to monzosyenitic intrusions, the Biella and Traversella plutons, near the Sesia-Ivrea contact (Fig. 5.1). These shallow intrusions (ca. 5 km intrusion depth, Rosenberg 2004 and references therein) are undeformed and clearly postdate all structures and metamorphism in the Mombarone unit (Babist et al., Chapter 4).

(2) the Bard unit occupies the Sesia Zone between the Mombarone unit (above) and the Piemont-Liguria ophiolites (Fig. 5.1). The Bard unit comprises

well-foliated, fine-grained biotite-albite-white mica-epidote gneiss with minor intercalations of chlorite-calcic amphibole gneiss and subordinate phengite-bearing quartzite. Evidence for HP metamorphism in the Bard unit is sparse (coronitic grt-cpx surrounding pre-Alpine granulite-facies paragenesis, Lardeaux and Spalla 1991) due to strong synkinematic and static greenschist-facies overprinting (Pognante et al. 1987; Lattard 1975; Compagnoni et al. 1977; Reddy et al., 1999, Lardeaux and Spalla, 1991). Peak pressures attained in the Bard unit are estimated to have been 1.0-1.5 GPa at 500-550°C (Lardeaux and Spalla 1991), whereas the later overprint occurred at about 0.5 GPa at 350-450°C (Pognante et al. 1987; Lattard 1975; Compagnoni et al. 1977; Reddy et al., 1999). Unfortunately, this strong overprint lead many workers to overlook the HP relics and therefore to doubt that the Bard unit ever experienced Alpine subduction (e.g., Pognante, 1989; Venturini, 1995; Ridley, 1989). Some even proposed a metamorphic field gradient ranging from eclogite facies in the Mombarone unit to greenschist facies in the Bard unit (e.g. Passchier et al., 1981; Williams and Compagnoni, 1983). As pointed out below, the occurrence of Mesozoic sediments between the Bard and Mombarone units (Fig. 5.1) and the contrast in peak pressures for HP assemblages in the two units preclude such a field gradient and support the original idea of Compagnoni et al. (1977) that the parts of the Sesia Zone corresponding to the Bard and Mombarone units are separate tectonic units.

(3) Sediments along part of the tectonic contact between the Bard and Mombarone units (Fig. 5.1) experienced only Alpine (i.e. post-Jurassic) metamorphism (Monometamorphic Cover Complex of Venturini 1995) and show a close affinity to Mesozoic metasediments separating basement units in other parts of the Alps. In addition, they have metabasic and metacarbonate rocks, mainly MORB-like metabasalts associated with several gabbroic lenses and mica-bearing marbles that contain upper blueschist- to eclogite-facies assemblages (Venturini, 1995). We therefore use these sediments as convenient markers to distinguish the Bard and Mombarone basement units, which we argue elsewhere (Babist et al., Chapter 4) were juxtaposed during Late Cretaceous nappe stacking and early exhumation. The sediments attained peak metamorphic pressures of 1.2-1.5 GPa at 500 to 550°C (Venturini, 1995), i.e., somewhat lower than the peak pressures tin HP rocks of the Mombarone unit, but similar to those attained in the Bard unit.

(4) Two elongate bodies of pre-Alpine granulite- and amphibolite-facies schist and gneiss, as well as several smaller lenses of gabbro and peridotite (Dal Piaz et al., 1971; Lardeaux et al. 1982) exist within the Bard unit and at its contact with the Mombarone unit (Fig. 5.1). These bodies are known in the local literature as the Seconda Zona Dioritica Kinzigitica (II ZDK, e.g. Carraro et al., 1970; Dal Piaz et al., 1971) based on their affinity with pre-Alpine rocks of the Ivrea Zone. Pre-alpine metamorphic conditions were on the order of 700-800°C and 0.5-1.0 GPa (Lardeaux et al, 1982; Rebay and Spalla, 2001). Alpine blueschist-facies metamorphic overprinting only locally affects the mylonitic contact with the Mombarone unit (e.g. Compagnoni et al., 1977; Gosso, 1977; Stünitz, 1989; Ridley, 1989; Avigad, 1996, Babist et al., Chapter 4), whereas the Alpine greenschist-facies metamorphic overprint can be found in the smaller lenses as well as in parts of the two main II ZDK bodies (Figure 5.1; e.g. Dal Piaz et al., 1971; Isler and Zingg 1974).

5.3.2 Fabric domains

The juxtaposition of the units above is intimately tied to their structural evolution as manifested by the distribution of Alpine fabric domains in the Sesia Zone, shown in Figure 5.2 (Babist et al., Chapter 4). Fabric domain 1 comprises a schistosity (S_1) formed under eclogite-facies conditions in the central part of the Mombarone unit. This schistosity is one of three upper blueschist- to eclogite-facies deformational phases which can only locally be distinguished (Zucali et al. 2002) and which developed before or during nappe stacking in the Sesia Zone. S_1 is overprinted in fabric domain 2 under retrograde blueschist- to greenschist-facies conditions (Zucali et al., 2002; Babist et al., Chapter 4). This overprinting involved mylonitic shearing (S_2 schistosity) and isoclinal folding (Williams and Compagnoni, 1983; Gosso, 1977; Zucali et al., 2002), and is most intense along part of the steeply NE-SW trending nappe contact of the Mombarone and Bard units (Fig. 5.2).

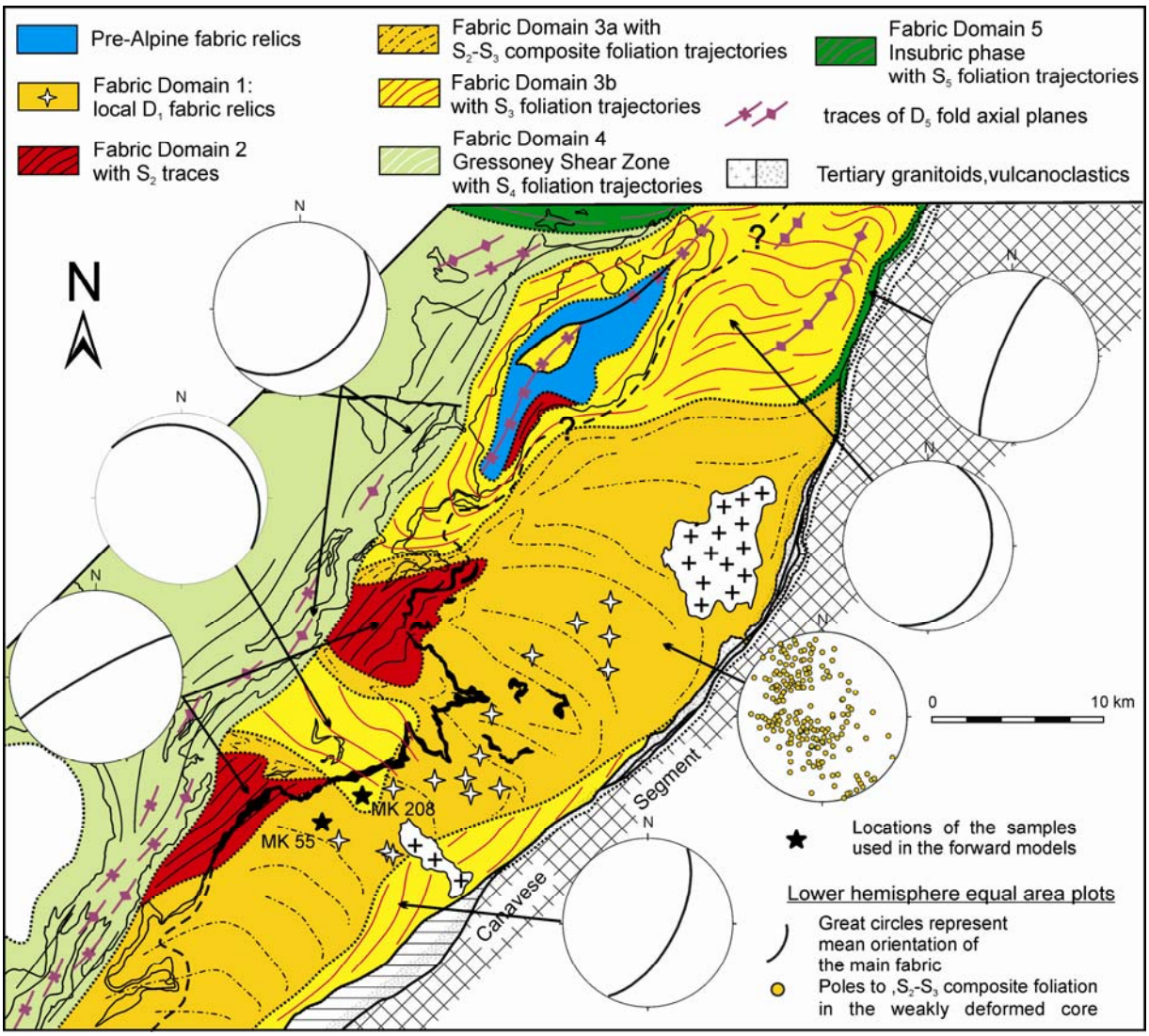

Fig. 5.2: Fabric domains in the central Sesia Zone (modified after Babist et al., this volume). The trajectories display the trace of the main foliation. Stereoplots show great circles of the main foliation and are lower hemisphere projections. Additionally shown are the locations of the samples used in the forward models. See text for further discussion.

Fabric domains 3a and b are characterized by meter- to multimeter-scale isoclinal folds whose subhorizontal axial plane schistosity is transitional to a greenschist-facies mylonitic foliation (S_3) in the structurally highest parts of the Sesia Zone (Fig. 5.2). This foliation accommodated top-E to -SE normal faulting in both the Bard and Mombarone units (Babist et al., Chapter 4). The retrograde overprint in fabric domain 3a is often strong in a structural sense but only weak in a metamorphic sense (Zucali et al., 2002) in that HP assemblages are well preserved in the Mombarone unit. Fabric domain 4 marks the aforementioned Gressoney Shear Zone, which effected top-SE, greenschist-facies mylonitic shearing of the Bard unit and the underlying Piemont-Liguria ophiolites in Early

to Mid Tertiary time (Wheeler and Butler 1993; Reddy et al., 1999). Fabric domain 5 comprises strands of greenschist-facies mylonite and upright, acylindrical folds at the western end of the Oligo-Miocene Periadriatic fault system (Schmid et al., 1987; Zingg and Hunziker, 1990; Handy et al. 2005). These shear zones accommodated SE-directed backthrusting of the Sesia Zone onto the Ivrea Zone, as well as dextral transpressional shearing of the Late Cetaceous to Early Tertiary nappe stack with respect to the cool and rigid, southern Alpine units (Fig. 5.1). Numerous cataclastic fault zones overprint these shear zones but are beyond the scope of this paper.

We note that the fabric domains overprint the boundaries between all four lithotectonic units (Fig. 5.2) and that the Bard and Mombarone units attained different peak pressures. This indicates, first, that the primary nappe contact of the Bard and Mombarone units developed after the attainment of peak HP conditions, but prior to or during D_1 deformation (Babist et al., Chapter 4), certainly prior to D_2 shearing. The nappe contact is therefore the only large, subduction-related structure preserved in the Sesia Zone. Second, fabric domains 3 to 5 formed within continental crust and must have occurred after the crust was exhumed from mantle depths to the base of the upper plate. This feature becomes important when assessing the retrograde P-T paths of the eclogitic rocks in terms of exhumation mechanisms.

5.4 RESULTS OF THERMOBAROMETRY AND THERMODYNAMIC MODELLING

5.4.1 Approach and assumptions

To assess the roles of fractional crystallisation and water fractionation during exhumation, we used the THERIAK algorithm (de Capitani and Brown, 1987; Konrad-Schmolke et al., 2005) to calculate P-T paths that reproduce observed chemical zonation patterns in retrograde minerals for fabric domains 2 and 3. These paths are then compared with P-T paths derived from conventional thermobarometry on the same mineral parageneses using P-T-X pseudosections and amphibole thermometry (Holland and Blundy, 1994; solution models given in the Appendix). The path which best fits both the observed chemical zonation patterns and the thermobarometrically derived P-T path is then interpreted to yield information on the conditions of exhumation. Implicit in this approach is that the

mineral parageneses used for the calculation attained equilibrium during the main deformational event in their respective fabric domains.

To calculate a P-T path, a given P-T segment is divided into regularly spaced P-T increments for which the thermodynamic properties of the rock, e.g. mineral abundances, compositions and water content, are calculated. Fractional crystallisation and water fractionation are modelled by removing elements incorporated into the fractionated phases at each increment according to the method described in Konrad-Schmolke et al. (2005). We modelled exhumation along three different retrograde P-T paths each for fabric domains 2 and 3. These fabric domains are associated, respectively, with transpressional and extensional exhumation of the Mombarone unit during Late Cretaceous to Early Tertiary time (Babist et al., Chapter 4). All calculated retrograde paths are based on a common prograde path in order to account for the possible effects of prograde water- and mineral-fractionation, as outlined in Konrad-Schmolke et al. (2005). The prograde path starts at 400°C and 0.5 GPa, and ends at 550°C at 1.8 GPa, with the peak values taken from Zucali et al. (2002) for eclogite-facies conditions in the Mombarone unit.

Two different water fractionation scenarios are modelled for each P-T path: (1) water present in excess during all calculated steps; and (2) water produced by devolatilisation reactions is removed from the rock at each P-T increment (dehydration conditions).

5.4.2 Conditions during transpressional exhumation (fabric domains 1 and 2)

Retrogression of the eclogitic mineral assemblage is manifest by a strong decrease in omphacite abundance and the formation of new sodic amphibole, epidote and albite, as found in weakly D_2-deformed rocks from the central part of the Mombarone unit. Figure 5.3a shows sample MK 55, a metagranitoid rock with the partly preserved HP assemblage: garnet-sodic amphibole-phengite-omphacite-epidote/zoisite-rutile-paragonite-quartz. Omphacite and paragonite are locally replaced by albite, epidote and phengite (fine-grained pseudomorphs; arrow in Fig. 5.3a). The change in omphacite abundance is related to localised growth of Fe-rich sodic amphibole or to chemical re-equilibration of amphibole grains that were already present along grain boundaries (Figs. 5.3b and c).

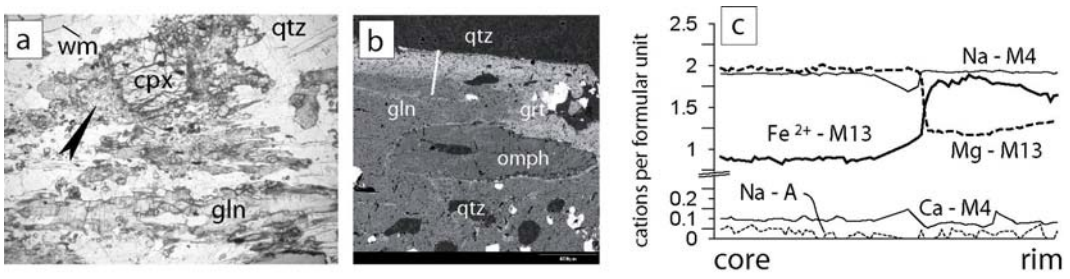

Fig. 5.3: a) Thin section photograph of a weakly D_2 deformed sample. The breakdown of omphacite is associated with the growth of epidote (arrow) as well as Fe-rich sodic amphibole (gln); wm=white mica. b) Back scattered electron image of a sodic amphibole with numerous inclusions of garnet (grt), omphacite (omph) and quartz (qtz). The lighter rims show the modification of the amphibole composition along the outermost rims. The line shows the position of the compositional profile shown in c).

These amphibole grain boundaries show a pronounced enrichment in Fe^{2+} associated with a decrease in Mg at the inner rim. Towards the outer rim this trend is inverted and Fe decreases continuously. Small grains of calcic amphibole and chlorite are observed at the tips of the sodic amphiboles. The pseudosection and isopleth pattern for the Fe content in sodic amphibole in Figure 5.4a is calculated for the bulk rock composition of this sample assuming a water- and quartz-saturated system containing the elements Na, Ca, K, Fe, Mg, Al, Si, H, O and Mn (NCKFMASHMn). The isopleth pattern shows an elongate maximum of Fe content aligned parallel to the Fsp-in isoline. Toward higher pressures at eclogite facies conditions, the Fe content decreases continuously from 0.6 to 0.4. Toward lower pressures, the Fe content rapidly decreases toward the zero mode line of sodic amphibole.

In the following calculations we modelled amphibole growth in the same sample along three different segments of the exhumation path. Path 1 involves continuous cooling during decompression to 0.8 GPa and 500°C, path 2 is characterised by isothermal decompression to 1.0 GPa followed by cooling to 500°C and path 3 involves heating to 600°C at 1.5 GPa followed by continuous cooling during decompression (Fig. 5.4). The calculated increments are labelled on the P-T trajectories in Figure 5.4b.

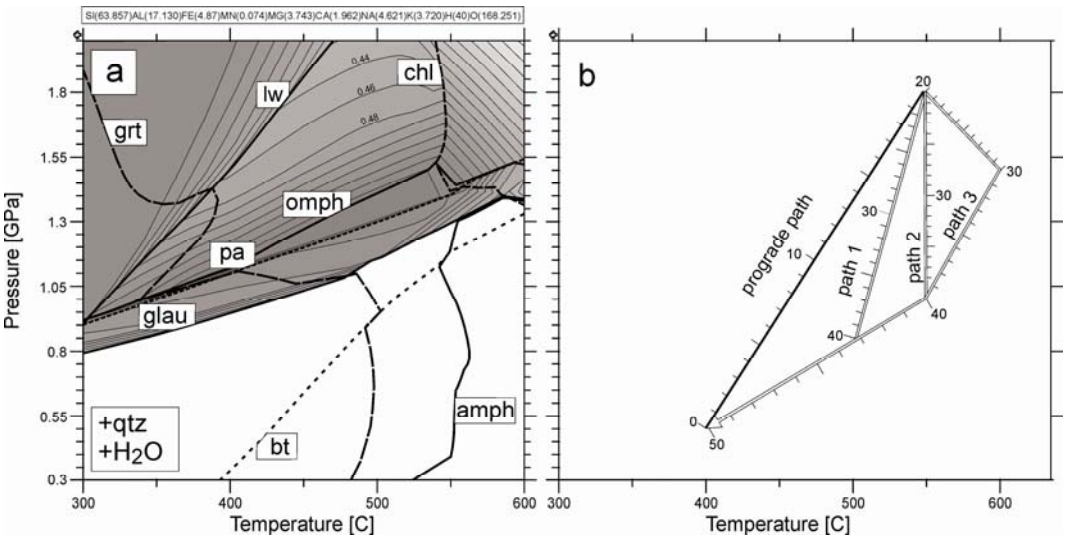

Fig. 5.4: a) Pseudosection and Fe-glaucophane isopleths calculated for the sample shown in Fig. 5.3. The zero mode lines are labelled such that the mineral abbreviation is shown on the "present" side. Darker colours indicate higher values. b) Three different calculated P-T paths and indicated P-T increments. Each retrograde P-T path follows a straight prograde path as shown in the diagram.

The diagrams in Figures 5.5 a-c show the calculated abundances of the NCFMASH-phases, excluding quartz and water, along the three retrograde P-T trajectories that involve fractional garnet crystallisation and water fractionation. The decrease in omphacite (omph) and paragonite (pg) accompanied by the increase in sodic amphibole (gln), epidote (ep) and feldspar (fsp) in the natural sample are successfully predicted by the forward model starting at P-T increment 28, at a pressure of 1.5 GPa. Although differences in the phase relations between the three model P-T paths are only minor (Fig. 5.5a-c), the compositional evolution of sodic amphibole depends strongly on the shape of the P-T path. In contrast to the calculations along paths 1 and 2 (Fig. 5.5a and b), the ferroglaucophane (Fe-Gln) content in sodic amphibole steadily decreases in the calculations along path 3 (Fig. 5.5c). For path 3, an increase in Fe content associated with the formation of sodic amphibole is hindered by the formation of retrograde garnet (grt) and albitic feldspar. The resulting zonation pattern shows steadily decreasing glaucophane (gln)- and increasing ferroglaucophane (Fe-gln)-contents during decompression. This contrasts with the observed chemical zonation of sodic amphibole in the sample. Thus, the zonation pattern of sodic amphibole indicates that the retrograde P-T trajectory for initial exhumation (D_1 and D_2) is characterised by isothermal decompression or cooling.

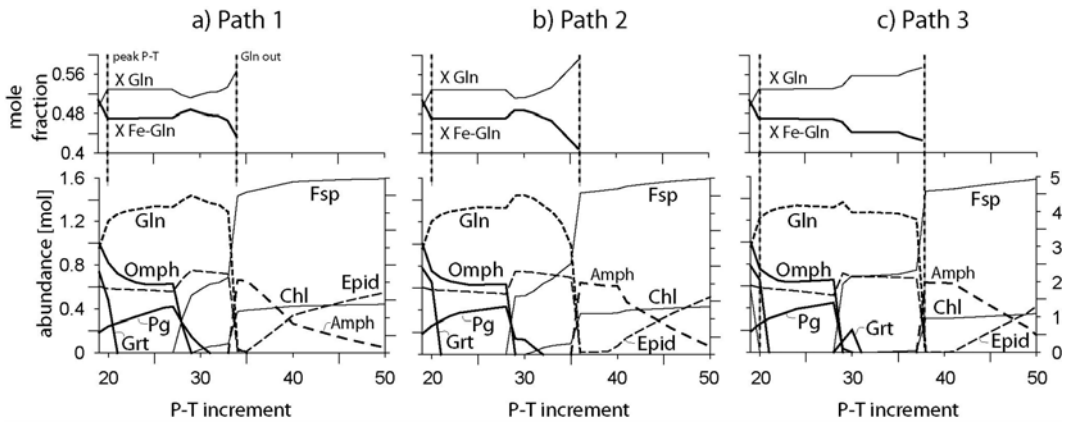

Fig. 5.5: Mineral abundances and sodic amphibole composition modelled along the three different P-T trajectories for the sample shown in Fig. 5.3 (see text). a) Path 1: decreasing temperatures during decompression; b) path 2: isothermal decompression; c) path 3: heating during decompression. Abundances of sodic amphibole (gln), omphacite (omph) and feldspar (fsp) are plotted on the right axis.

The influence of water content in the system during this initial retrograde evolution is shown in Figure 5.6a. The mineral abundances as well as the sodic amphibole composition in this plot are calculated along path 2, where it is assumed that water is present in excess at every calculated increment. Interestingly, the difference between the calculations assuming continuous dehydration and those assuming excess water are only minor, indicating that the amount of water in hydrous phases in these rocks is still sufficiently high to enable the retrograde phase transitions observed in this sample.

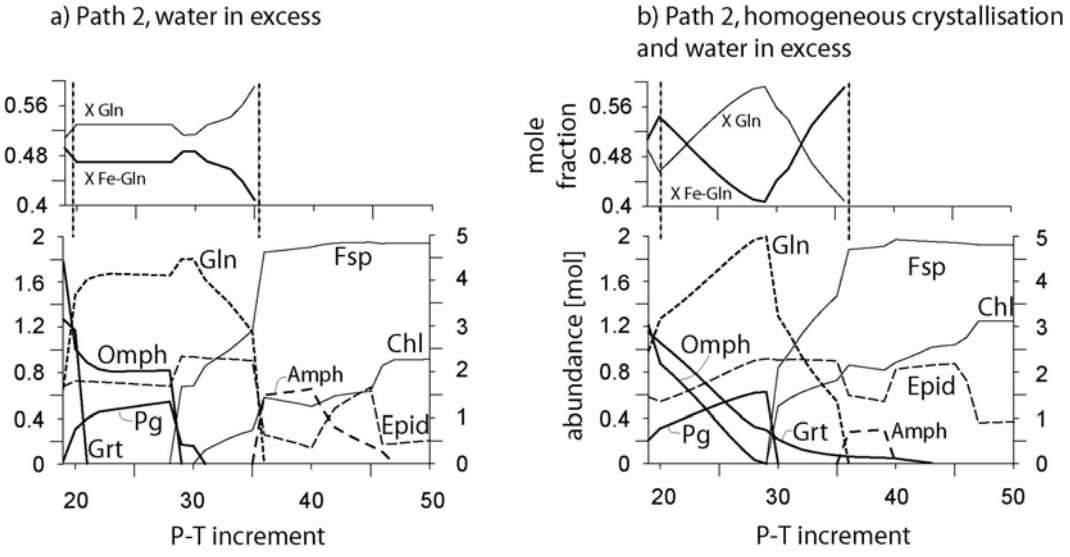

Fig. 5.6: Mineral abundances and sodic amphibole composition modelled along path 2 for the same sample, but water present at all calculated steps (a) and additionally homogeneous garnet crystallisation (b).

In contrast, fractional garnet crystallisation significantly influences the compositional changes of sodic amphibole, as shown in Figure 5.6b, which was calculated by assuming homogeneous equilibrium crystallisation and water present in excess at every calculated step.

A very common feature in these rocks is the modification of phengitic white mica to more Si- and Fe-rich compositions at the rims and the associated formation of K-feldspar along white mica grain boundaries (BSE images in Figs. 5.7a and b). Figure 5.7c shows the change in mica composition along the line indicated in Figure 5.7b in a sample with similar bulk rock composition and from the same outcrop as the previous sample. Although mica composition is known to depend strongly on the coexisting mineral assemblage (e.g. Massonne and Schreyer, 1987), the $Al^{IV}Al^{VI}\_Si^{IV}Fe^{VI}$ (Tschermak-) substitution in white mica is commonly interpreted to reflect increasing pressure.

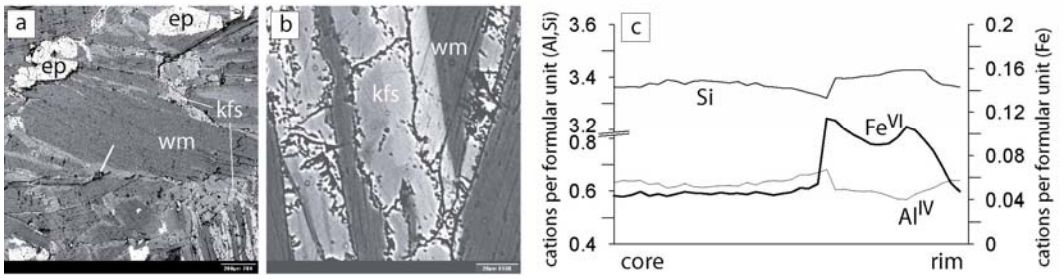

Fig. 5.7: Modified white mica composition in a sample from the same outcrop. a) and b): BSE images showing the strongly modified grain boundaries and the phase relations between white mica and K-feldspar. The line marks the position of the compositional profile shown in c).

But the pseudosection calculated for the bulk rock composition of this sample shows that the Si-isopleths are strongly distorted in the phase fields that contain albitic feldspar with another Na-bearing phase, such as omphacite and sodic amphibole (Fig. 5.8). This effect is amplified by fractional crystallisation, as seen in the Figures 5.9a-c. These diagrams show the modelled mineral abundances as well as the composition of white mica along the three P-T paths. The formation of retrograde K-feldspar associated with increasing Si^{IV}- and Fe^{VI}-content in white mica can be seen in paths 1 and 2. In contrast, this increase is virtually absent for calculations in which temperatures increase during initial decompression (path 3).

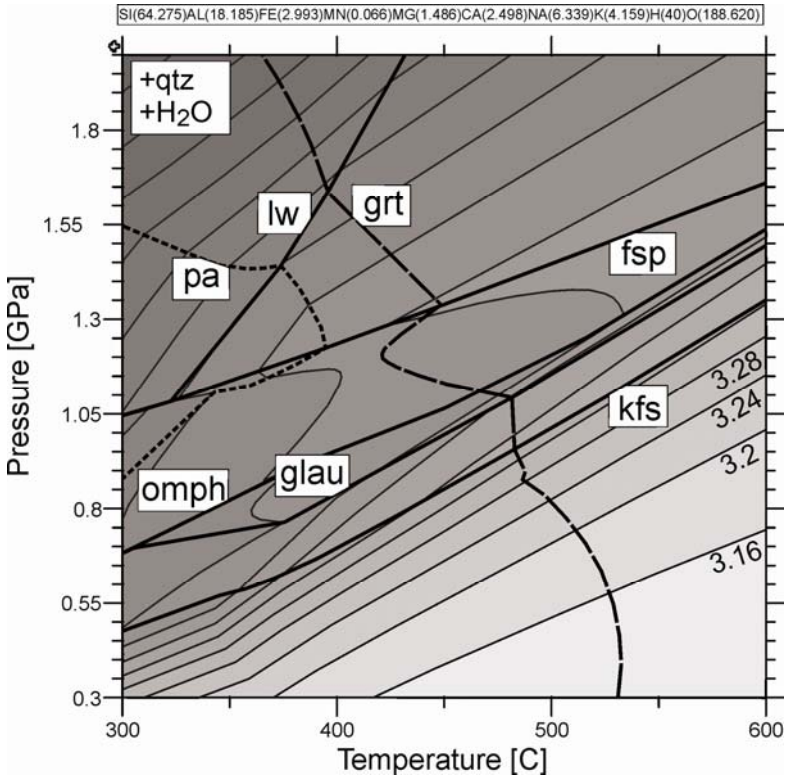

Fig. 5.8: Pseudosections and Si-isopleths calculated for the sample in Fig. 5.7. The isopleths are strongly curved in the phase fields containing albitic feldspar and another Na-bearing HP phase. This might lead to increasing Si content in white mica during decompression.

The white mica composition is modified by the decrease in omphacite between points 27 and 31, at pressures between 1.5 and 1.35 GPa. Interestingly, increased celadonite content in white mica is associated with decreasing pressures, as shown above.

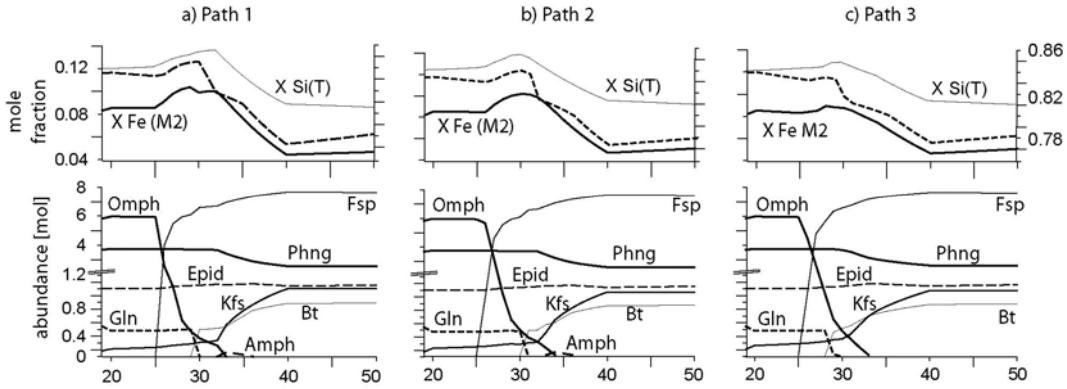

Fig. 5.9: Mineral abundances and white mica composition calculated along the P-T trajectories shown in Fig. 5.4, assuming fractional garnet crystallisation and water fractionation. The stippled lines in the compositional diagrams show the modelled change in XFe composition assuming water in excess at all calculated steps. XSi on right axis.

The presence or absence of water does not significantly influence the composition of white mica. This is shown by the stippled lines in the mica compositional diagram in Figure 5.9 that displays the Fe^{VI}-content assuming water present in excess at every calculated step.

5.4.3 Conditions during extensional exhumation (fabric domain 3)

Figure 5.10a shows a photomicrograph of a metabasic rock (MK 208) sampled in a strongly refolded part of the D_2 shear zone between the Bard and Mombarone units in the southern part of the Sesia Zone. The sample preserves a well-developed S_2 foliation defined by omphacite, sodic amphibole chlorite and zoisite that wrap around large pre-D_2 garnet clasts. These clasts have prograde chemical zonation patterns and numerous rutile inclusions indicative of a high-pressure origin. In addition, phengitic mica and blue-green calcic amphibole, often overgrown on sodic amphibole (Fig. 5.10b), are aligned parallel to S_2 and therefore belong to the D_2 mineral assemblage. The deformation of S_2 by F_3 folds is associated with the breakdown of omphacite and sodic amphibole to form chlorite, green and colourless calcic amphibole, epidote and albitic feldspar. This is most pronounced in high-strain structures such as F_3 fold limbs and shear bands (Fig. 5.10c).

The two types of calcic amphibole in this sample have different characteristics: (1) medium-grained pargasitic hornblende with increasing Na-content towards the grain rims are aligned parallel to the refolded S_2, mainly in the vicinity of sodic amphibole (Fig. 5.10b); (2) fine-grained Na-poorer calcic amphiboles with tremolitic to magnesio-hornblende compositions sometimes have a chemical zonation of decreasing pargasite- and increasing tremolite-component from core to rim. Such grains occur throughout the sample, especially in areas that experienced strong D_3 deformation (Fig. 5.10c). The chemical zonation patterns representative of the two amphibole generations are shown in Figures 5.10d and e. These patterns can be used to determine the slope of the P-T path for D_3 extensional exhumation.

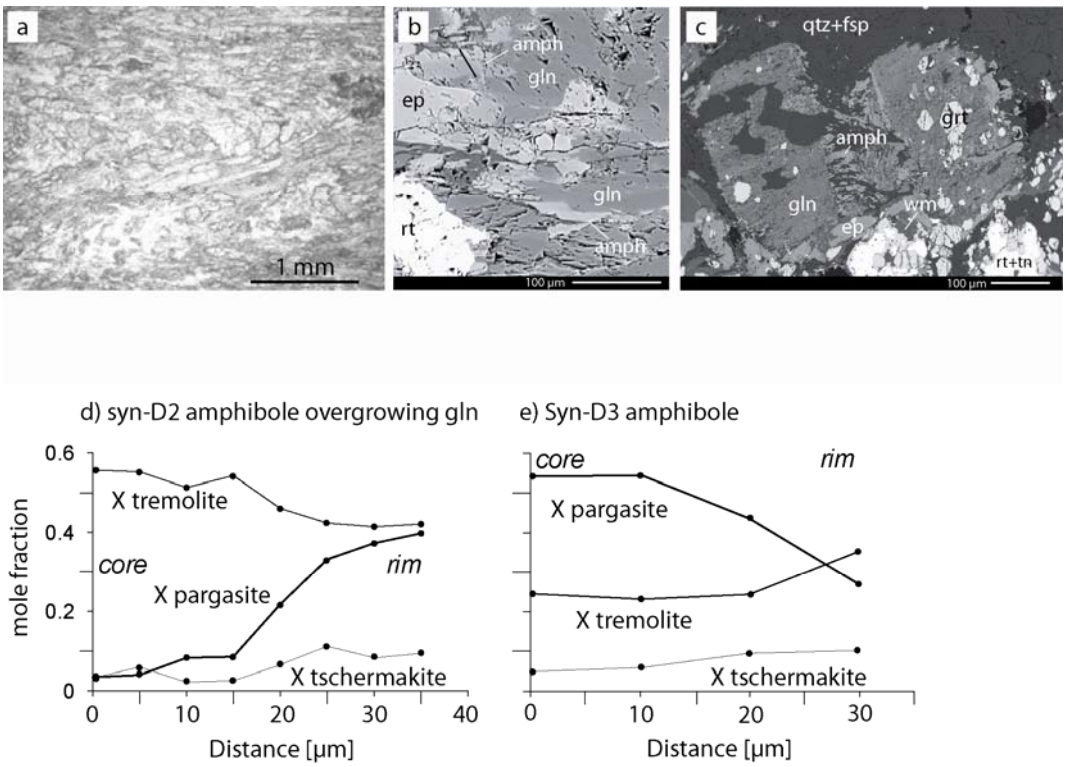

Fig. 5.10: a) thin section photograph of a syn-D_3 refolded metabasite preserving a strong S_2 foliation defined by omphacite, sodic amphibole (with overgrown calcic amphibole) and epidote. Fine grained matrix amphibole can be found aligned parallel to the axial planes of the F_3 folds; b) BSE image of calcic amphibole overgrowth on sodic amphibole aligned parallel to the S_2 foliation. The black line marks the position of the compositional profile in d). c) Syn-D_3 boudinaged sodic amphibole grain with newly formed synkinematic calcic amphibole in the neck. d) Compositional profile across the calcic amphibole overgrowth in b). e) Compositional profile across a fine-grained syn-D_3 calcic amphibole from the same sample

As above, we calculated three retrograde P-T paths, each with different slopes, but each following from the near-isothermal decompression P-T path derived for initial exhumation. The resulting chemical zonation patterns were then compared with the observed amphibole zonation patterns to constrain the D_3 exhumation path.

Calcic amphibole composition has characteristic trends along the P-T paths that are shown as insets in Figures 5.11a-c. For calculations involving heating during further decompression, calcic amphibole shows a continuously increasing pargasite component associated with a rapidly increasing tschermakite component (Fig. 5.11c), even in the absence of sodic amphibole.

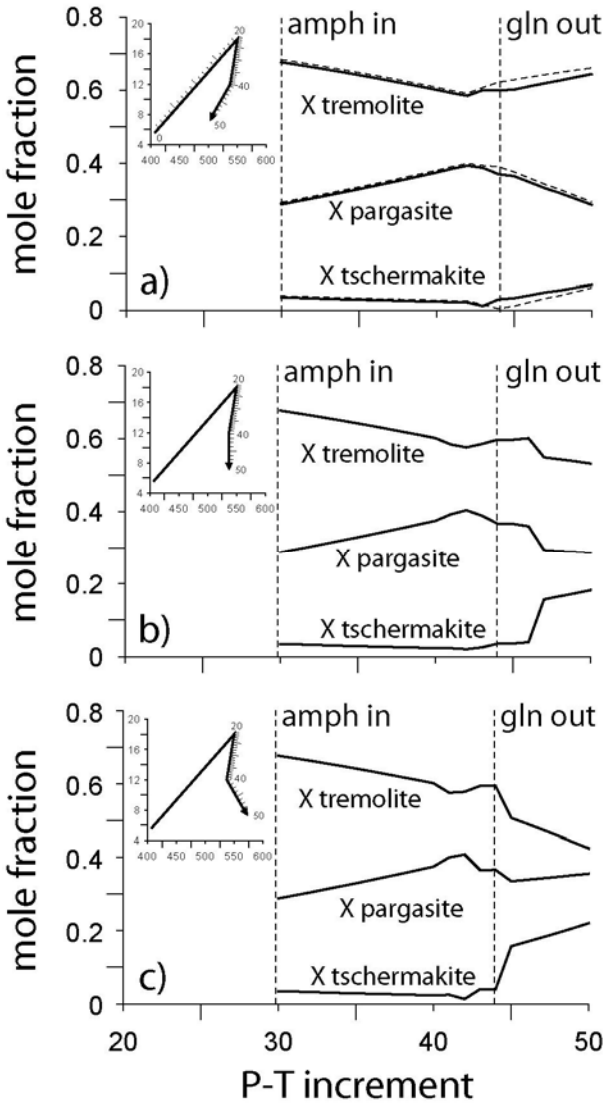

Fig. 5.11: Calculated amphibole composition along the modelled P-T trajectories shown in the insets. Mark the differences in amphibole composition beyond the stability of sodic amphibole.

In contrast, models involving constant or decreasing temperature during decompression predict a characteristic change in the compositional trend of calcic amphibole from increasing to decreasing pargasite component at the zero mode line of sodic amphibole. Opposite trends are predicted for tremolite and tschermakite contents (Figs. 5.11a and b), as observed in the two amphibole generations in this sample. Amphibole grown in the presence of sodic amphibole shows increasing pargasite and decreasing tremolite contents (Fig. 5.10d), whereas matrix amphibole that experienced intense D_3 deformation shows the opposite trend (Fig. 5.10e). Therefore, the characteristic chemical zonation patterns of the two calcic amphibole generations clearly indicate that

decompression of the HP rocks to pressures of about 0.8 GPa is associated with cooling. It is remarkable that even at greenschist-facies conditions, the amphibole composition varies only slightly between models for water-saturated conditions (stippled lines) and those involving water fractionation (Fig. 5.11a). The effect of a free hydrous fluid phase on the mass balance of retrograde phase transitions at upper greenschist-facies conditions is apparently very limited in these rocks.

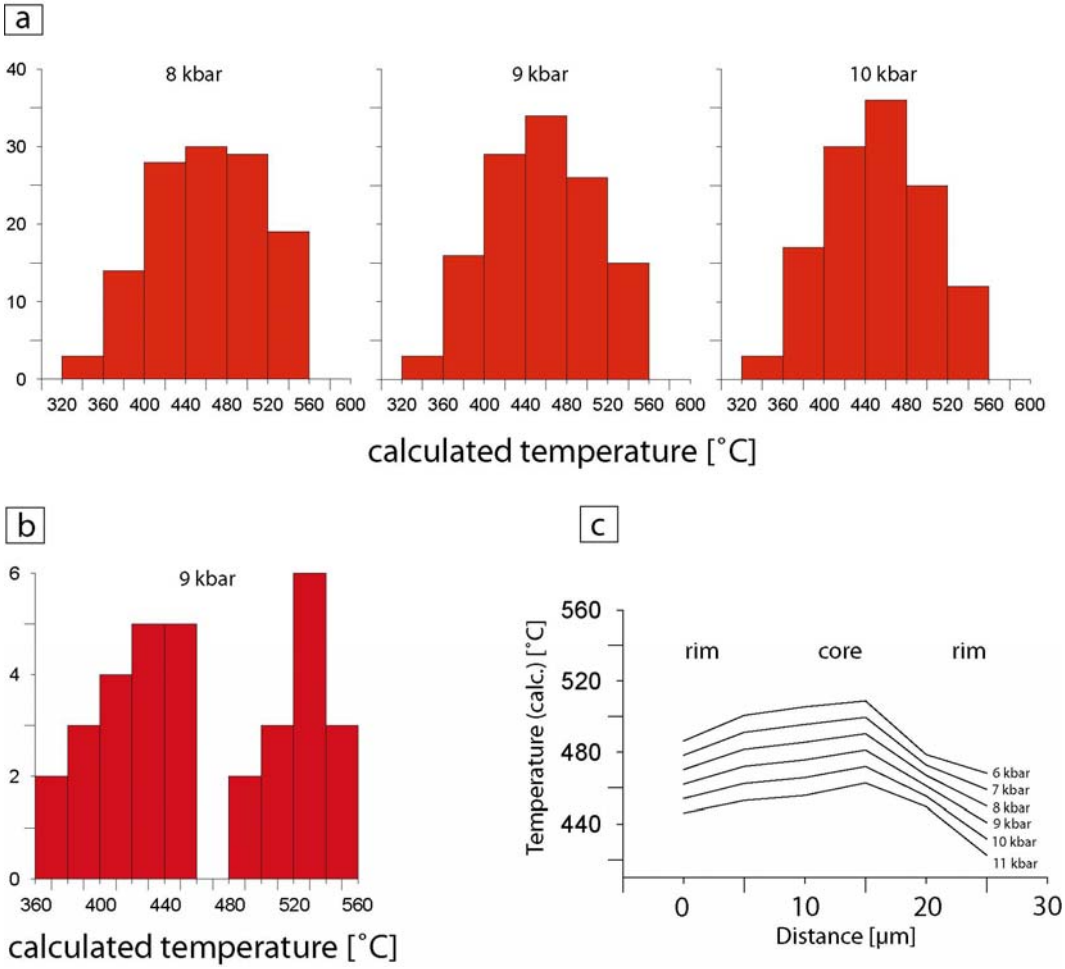

Fig. 5.12: a) Histograms showing the calculated temperatures for syn-D_3 calcic amphiboles using the edenite-tremolite-albite-quartz equilibrium and the calibration of Holland and Blundy (1994). b) Calculated temperatures for the two amphibole generations in the sample shown in Fig. 5.10. The higher temperatures are calculated for the overgrowths on sodic amphiboles, the lower temperatures are calculated for matrix amphibole. c) Calculated temperatures for a chemically zoned syn-D_3 calcic amphibole grain.

The temperatures obtained from the forward modelling of the calcic amphibole zonation patterns are consistent with estimates from amphibole thermometry using the edenite-tremolite-albite-quartz equilibrium and the calibration of Holland and Blundy (1994). The histograms in Fig. 5.12a show calculated temperatures for 125 amphibole analyses from 6 samples from the D_3,

top-E normal fault. Although the calculated temperatures range broadly (550°C to about 350°C), they cluster about 460°C irrespective of the assumed pressures. These values are significantly lower than the D_2 temperatures obtained from the forward models above. This is corroborated by the temperatures calculated from D_2 and D_3 calcic amphiboles in the sample shown in Figure 5.10a. The histogram in Fig. 5.12b clearly shows a bimodal distribution of calculated temperatures, with the maxima at 530°C and 440°C corresponding, respectively, to D_2 pargasitic amphiboles and new D_3 amphiboles. Calculations for the chemically zoned amphiboles in Figure 5.10e indicate decreasing temperatures during amphibole growth (Fig. 5.12c). Interestingly, amphiboles formed during Gressoney extensional shearing of the Bard unit (fabric domain 4 in Fig. 5.2) yielded temperatures of about 460°C, only slightly lower than those obtained from D_3 amphiboles. Nevertheless, both forward modelling and conventional thermobarometry indicate that extensional exhumation of the Sesia Zone involved pronounced cooling during decompression.

5.5 DISCUSSION

5.5.1 Interpretation of forward thermodynamic modelling in terms of a P-T path

Most thermodynamic modelling is conducted on garnet because diffusion in garnet is sufficiently slow to preserve growth zonation patterns (e.g. Spear, 1993 and references therein), even at high metamorphic temperatures. However, due to the low geothermal gradients in subduction zones, chemical zonation patterns can also be preserved in HP minerals with higher diffusivities, such as amphiboles and micas. This allows a comparison of zonation patterns in different minerals from the same sample and therefore provides an independent, internally consistent test of their interpretation in a geodynamic context (e.g. growth zonation patterns in sodic amphibole and white mica in Figures 5.5 and 5.8). The examples in Figure 5.6 clearly show the significant influence of fractional garnet crystallisation and the resulting change in the reacting bulk chemistry on the composition of sodic amphibole. Although the compositional changes due to water fractionation are minor in these samples, growth zonation patterns in garnets can be interpreted in terms of the amount of a fluid phase available during metamorphism (Konrad-Schmolke et al., Chapter 3). Mahar et al. (1998) showed

that fractionation effects significant changes in the topology of phases in petrogenetic grids, and must therefore be considered in thermodynamic calculations, especially in low temperature rocks. Although thermodynamic formulations of the solution models of most metamorphic minerals are inadequate to determine well-constrained, absolute values of pressure and temperature, they are sufficiently precise to detect changes in pressure and temperature during the metamorphic evolution. Knowledge of the relative values of pressure and temperature allows one to fill gaps between P-T estimates from conventional thermobarometry and thus to obtain information about segments of the P-T trajectory that are inaccessible with conventional thermobarometry (Fig. 5.13).

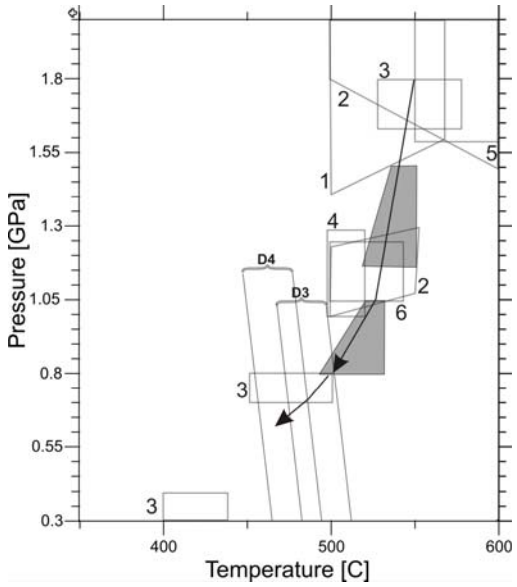

Fig. 5.13: Retrograde P-T trajectory of the Sesia Zone derived from the combination of thermodynamic forward modelling (dark shaded areas) and conventional thermobarometry. The thermodynamic models can give constraints on P-T segments that are poorly defined by conventional thermobarometry. (1: Pognante (1989); 2: Zucali et al. (2002); 3: Lardeaux et al. (1982); 4: Ridley (1989); 5: Tropper et al. (1999); 6: Williams and Compagnoni (1983).

5.5.2 The role of buoyancy in driving exhumation

Buoyancy-driven exhumation has been proposed for several UHP and HP terranes, including the Western Gneiss region in Norway (e.g. Walsh and Hacker, 2004), the Dabie Shan of China (Hacker et al., 1995), Crete (Thomson et al., 1998), the Tauern eclogites of the Eastern Alps (England and Holland, 1979), continental and oceanic units of the Penninic nappes in the Western Alps (Kurz and Froitzheim, 2002) and the Sesia Zone (Ernst, 1971). Buoyancy also plays an important role in driving exhumation of subducted crustal materials in most

numerical and analogue models of Alpine-type orogens (e.g. Chemenda et al., 1995; Burov et al., 2001).

Some workers have cited structures indicative of subvertical shortening and lateral extension as indirect evidence for buoyant rise of the lithosphere (Hacker et al., 1995; Ernst, 2001). Indeed, subvertical shortening in several of the UHP and HP terranes cited above has been attributed to an abrupt decrease in buoyancy of the HP rocks as they reach the crust-mantle transition (e.g. Walsh and Hacker, 2004). Yet, structural criteria for determining the role of buoyancy in exhumed HP terranes are ambiguous. For example, the low-angle normal faulting, vertical shortening and pronounced cooling recorded in fabric domain 3 of the Sesia Zone (Fig. 5.2) may have been caused by forces other than buoyancy, for example, gravitationally induced flow within the overthickened part of a crustal wedge, similar to the scenario envisioned by Platt (1986) for syn-orogenic extension of the Tertiary Alpine nappes.

Two factors play complementary, yet competing roles in buoyancy-driven exhumation of HP rocks: For a subducted rock body to rise, the buoyancy forces acting on this body must be large enough to exceed the shear strength of the deforming rock at its interface with surrounding rocks. Because buoyancy is primarily a function of a rock's volume and density contrast with the surrounding material, larger low-density rock bodies develop greater, upwardly directed buoyancy forces. On the other hand, the buoyancy forces acting on a large rock body cannot be so large that the slab rises quickly, retaining its heat and facilitating retrograde re-equilibration of the HP mineral assemblage at shallow depths. Thus, there must be an optimal combination of density contrast, rock volume and shear resistance that allows HP assemblages to be preserved during buoyancy-driven exhumation.

To determine the feasibility of buoyancy-driven exhumation of HP rocks in the Sesia Zone, we extract information on mineral densities and molar volumes from our thermodynamic models above to determine the density contrast between the HP rocks and their surrounding rocks at every calculated step of exhumation along the retrograde P-T path for the Mombarone unit (Fig. 5.14). To construct Figure 5.14, we assume the average composition of the exhuming rock body to be that of the Sesia Zone (50% metapelitic rock, 40% metagranitoid, 10% metabasic

rock, Compagnoni et al., 1977). The crustal thickness of the upper, Apulian plate at the time of Late Cretaceous subduction is taken to be 30 km. This value is very poorly constrained and represents a probable upper limit on the thickness of the shortened, distal Apulian passive continental margin. The upper plate lithosphere of this margin is assumed to have had a tripartite structure, similar to that presently exposed in the Ivrea Zone (upper mantle: 3.25 g/cm^3, mafic granulitic lower crust: 2.95 g/cm^3, quartz-rich upper crust: 2.75 g/cm^3).

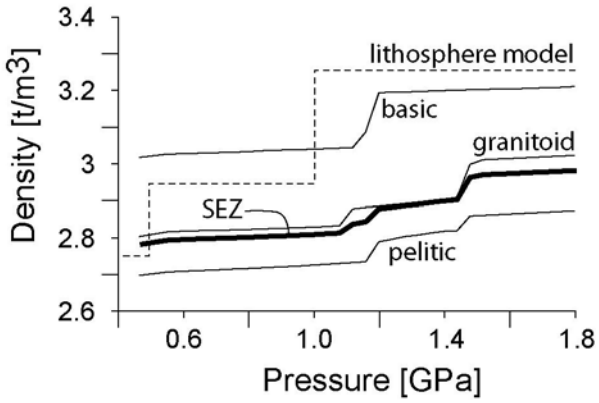

Fig. 5.14: Calculated densities of the subducted slab and the lithosphere according to the three-layer model used for the buoyancy calculations (see text).

Figure 5.14 depicts the calculated densities of the Sesia rocks along the retrograde P-T trajectory in Figure 5.13. The step-like decrease in density between 1.5 and 1.0 GPa is the result of mainly two reactions: (1) the replacement of omphacite in metapelitic and metagranitoid rocks by sodic amphibole and albitic feldspar between 1.5 and 1.2 GPa (calculations in Figs. 5.5 and 5.6); and (2) the breakdown of sodic amphibole at about 1.1 GPa. Together, these reactions increase the density contrast with the adjacent upper mantle rocks, thus enhancing buoyancy. Figure 5.14 also shows that for upper plate lithosphere with this tripartite layering, the Sesia Zone will lose its buoyancy as it passes from lower to upper continental crust.

To asses whether buoyancy generates shear stresses that are sufficient to overcome viscous shear resistance to upward motion of the Sesia rock body, we calculated shear stress versus depth in Figure 5.15 for different thermal gradients, deformation mechanisms and hydrous conditions of the rocks in the upper Apulian plate. The lithological structure of this plate is identical to that in Figure 5.14. For the sake of simplicity, we assume that the exhuming eclogitic rock body

is tabular, with areal dimensions like that of the Mombarone unit in cross-section (90 km length x 10 km depth, Babist et al. Chapter 4) and a variable average width (1, 5 and 20 km). The original dimensions of the exhuming body are obviously unknown and probably varied with deformation during exhumation. We note that although these dimensions correspond roughly to those of the Mombarone unit today, the results obtained below are robust and pertain generally to other large eclogitic bodies. Details of constructing the model in Figure 5.15 are outlined in the Appendix.

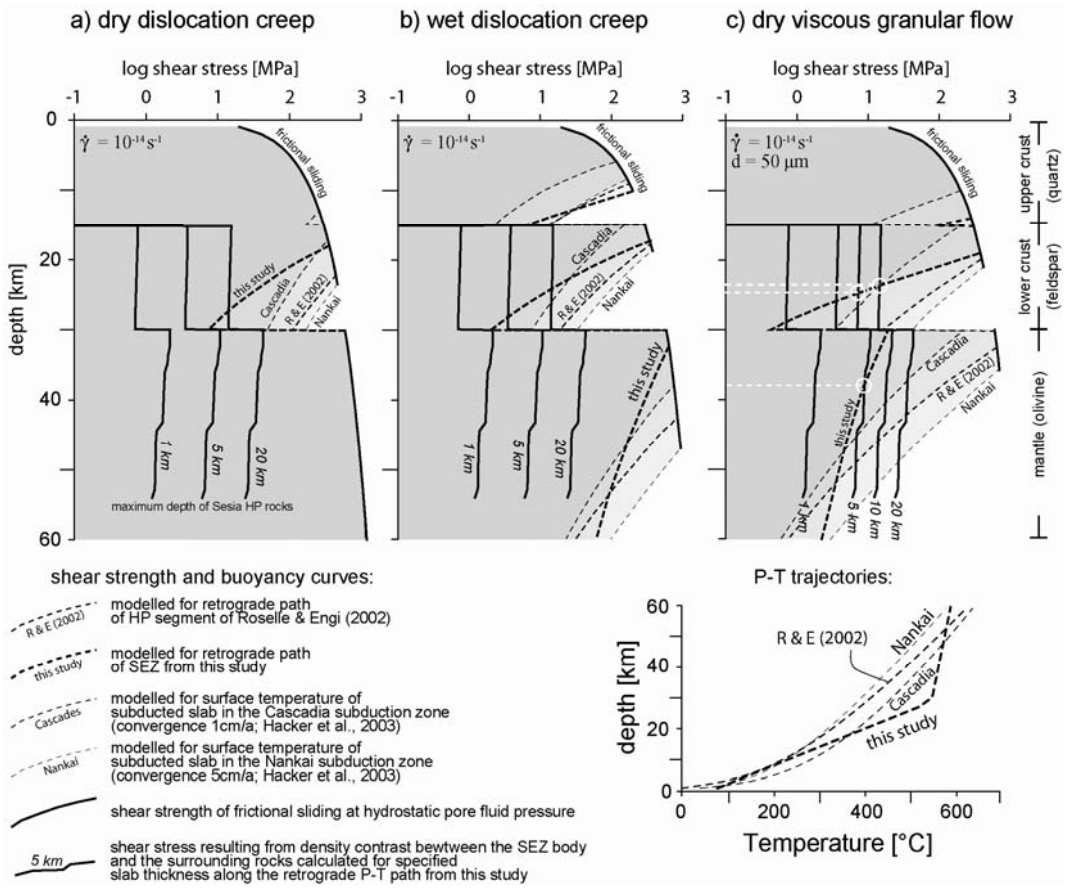

Fig. 5.15: a) Shear strength of the lithosphere model (stippled lines), assuming dry rocks and dislocation creep regime, calculated for four different thermal gradients (see inset). Additionally shown are the calculated shear stresses resulting from the density contrast between the SEZ and the surrounding rocks (solid lines) for specified widths of the exhumed tabular slice. Buoyant rise of the subducted slab is only possible if the resulting shear stresses exceed the strength of the lithosphere (see text for discussion); b) same calculations as in a), but with hydrated rocks; c) same calculations as in a), but assuming grain size sensitive viscous granular flow. The white circles and stippled lines mark the depths to which buoyant rise of a 5, 10 and 20 km thick SEZ slab is possible. References for creep parameters can be found in the appendix.

The 54 km depth of the diagrams in Figure 5.15 corresponds to the maximum subduction depth of the Sesia HP rocks, derived from pressure

estimates in the Mombarone unit (cited above). Temperatures of creep were calculated for a slab-parallel geothermal gradient derived from the P-T path (Fig. 5.13) of the exhuming Sesia rocks (curves labelled "this study"). For comparison, shear stress curves are included for rapidly (5cm/a, "Nankai") and slowly (1cm/a, "Cascadia") subducting slabs (Hacker et al., 2003), as well as for an exhumed sliver of continentally derived UHP rock modelled by Roselle and Engi (2002). The circles on the curves in Figure 5.15 mark depths where shear stress due to buoyancy is equal to the shear resistance of viscous creep to upward motion of the exhuming Sesia body. At depths below these circles, buoyancy-driven exhumation is possible within the given lithological domain because buoyancy-related shear stresses exceed the viscous shear strength of the adjacent rock.

It is evident from Figure 5.15a that in an anhydrous lithosphere even large slices of subducted continental rocks cannot buoyantly rise through the upper mantle, mostly because the shear strength of dry, olivine-rich rocks is several orders of magnitude higher than the shear stresses resulting from density contrasts between the exhuming HP body and its surrounding mantle rocks. Thus, other processes must weaken these mantle rocks to enable buoyancy-driven exhumation of subducted rocks from 60 km depth.

Figures 5.15b and c show that the shear strength of the surrounding rocks is significantly reduced by hydration and/or a change of the deformation mechanism from dislocation creep to grain size-sensitive, viscous granular flow. Although the shear strength of hydrated mantle rocks in Figure 5.15b still exceeds the buoyancy-induced shear stresses, the shear strength calculated for mantle rocks undergoing viscous granular flow in Figure 5.15c are sufficiently low to enable buoyant rise of a 10 km thick eclogitic body along the P-T path. In fact, in this example, buoyancy is predicted to drive the exhumation of HP body all the way up through the mantle and lowermost crust. Smaller syntectonic grain sizes, lower strain rates and/or hydrous conditions (not shown in Figure 5.15c) would reduce the resistance to buoyant exhumation even more, making it possible for even smaller eclogitic bodies to rise buoyantly.

A remarkable feature of the curves in Figures 5.15b and c is that buoyant exhumation of HP rock bodies is only possible along very steep, slab-parallel geothermal gradients, as calculated for the Sesia rocks in this study. The steepness

of this geothermal gradient reflects the nearly adiabatic conditions associated with near-isothermal decompression of the Sesia rocks during their initial, transpressional stage of exhumation. Interestingly, many other HP and UHP terranes are characterised by steep P-T trajectories during the early stages of exhumation (e.g. Central Alps: Meyre et al., 1999; Syros/Sifnos in the Aegean Sea: Trotet et al., 2001; Southern Japan: Matsumoto et al., 2003; Sulu: Nakamura and Hirajima, 2000; Kokchetav: Hermann et al., 2001). Some of these terranes show an amphibolite- or granulite-facies metamorphic overprint (Caledonian and Variscan HP rocks, e.g. Walsh and Hacker, 2004; O'Brien and Vrana, 1995), whereas others, like the HP rocks of the Sesia Zone, do not.

Considered in light of Figure 5.15, steep exhumational P-T paths offer a possible explanation of why HP assemblages are preserved, apparently despite the intense deformation of their surrounding rocks, whereas others experience thermal overprinting metamorphism. Heat advected by the rapid, adiabatic rise of buoyant, subducted bodies can induce thermal weakening of the surrounding rocks, in turn accelerating buoyant rise of the HP rock bodies and preventing re-equilibration of the HP mineral assemblages to ambient conditions of the surrounding upper mantle or lower crust. However, once the exhuming body reaches levels where its density contrast with the surrounding rocks decreases and/or where its rate of heat loss increases significantly, then the shear strength of the surrounding rocks is expected to increase while the buoyancy-induced shear stress decreases. This slows or even halts the exhumation, allowing heat to flow from the surrounding rocks of the overriding plate to the exhumed rock body. If the heat transferred is great, then the HP assemblages experience the amphibolite- or granulite-facies metamorphic overprint cited above. However, where heat transfer from the surrounding rocks is limited, no re-equilibration occurs and the exhumed rocks record a syntectonic metamorphic evolution from eclogite- to blueschist- to greenschist-facies conditions, as in fabric domain 2 of the Sesia Zone.

In the Sesia Zone, the absence of an amphibolite-facies overprint and the development of steeply dipping, retrograde blueschist- to greenschist-facies mylonitic shear zones (Babist et al., Chapter 4) suggest that transpressional exhumation during D_1 and D_2 was rapid until the SEZ rocks reached mid-crustal depths (ca. 25 km). Because this initial exhumation was nearly adiabatic, we infer that the viscous strength of the upper mantle and lower crust was significantly

reduced, either due to local heating of rocks adjacent to the rising body, or to syntectonic reaction (favouring reaction-enhanced weakening and viscous granular flow, Fig. 5.15c, e.g., Handy 1989). Similarly steep shear zones active under retrograde, lower amphibolite- to greenschist-facies conditions and associated with the exhumation of UHP rocks have been documented in the Dora Maira massif of the Western Alps (Michard et al., 1993) and the Dabie Shan (Hacker et al., 1995).

Continuous cooling during extensional exhumation of the Sesia HP rocks occurs along a P-T path which precludes buoyancy as a driving force for D_3 extensional exhumation (Fig. 5.15). This stands in strong contrast to recent numerical models of Alpine-type orogenesis which attribute exhumation to buoyant, diapiric rise of subducted crust within a low-viscosity upper mantle wedge, leading to thermal erosion and lateral thinning of the overlying upper plate (Burov et al. 2001). It also suggests that D_3 sub-vertical shortening in the footwall of the D_3 normal fault in the Sesia Zone is driven by forces other than buoyancy.

Syn-orogenic extension in basement units of the Western Alps has been described by several authors (Henry et al., 1993; Wheeler and Butler, 1993; Avigad et al., 1993; Ballèvre and Merle, 1993). Indeed, some workers have proposed Tertiary extension to be the main mechanism for exhuming HP rocks in the Sesia Zone and Piemont-Liguria ophiolites (Inger and Ramsbotham 1997; Reddy et al. 1999, 2003). Wheeler et al. (2001) argued that exhumation of Early Tertiary HP rocks in the Western Alps was related to orogen-scale extension in the roof of the subducting Penninic units. The setting they propose is similar to that produced in the analogue model of Chemenda et al. (1995). The reader is referred to Babist et al. (Chapter 4) for a discussion of this and other proposed mechanisms of extensional exhumation, but we point out here that the timing of deformational events recently compiled on the orogenic scale (Schmid et al. 1997, 2004) precludes orogen-wide crustal extension at this time. As proposed by Babist et al. (Chapter 4), we favour local extension of the upper Apulian plate above the rolling hinge of a NW-retreating subducted slab in Late Cretaceous time as the most likely scenario for late, extensional exhumation of the HP rocks in the Sesia Zone. This was proposed for the Alps some time ago (e.g. Handy 1996; Froitzheim et al., 1997) and has its modern-day analogue in the Tertiary exhumation of HP rocks in the Aegean Sea behind the S-retreating Hellenic-Crete

trench-arc system (Parra et al., 2002; Jolivet et al., 2004 and references therein). However, we emphasize that most exhumation of the HP rocks in the Sesia Zone preceded Early Tertiary extension and was driven by buoyancy-forces during sinistral transpression between Europe and Apulia in Late Cretaceous time (Babist et al., Chapter 4).

5.6 CONCLUSIONS

Thermodynamic modelling of the chemical zonation patterns in HP minerals from the Sesia Zone reveals that nearly isothermal decompression (1.5 to 1.0 GPa at 500-550°C) during transpressional exhumation at retrograde eclogite- to blueschist- to greenschist-facies conditions was followed by pronounced cooling (500 to 400°C) and modest decompression (1.0 to 0.8 GPa) during extensional exhumation under hydrous greenschist-facies conditions. Modelling of synthetic P-T paths associated with chemical zonation patterns most similar to those observed in the natural samples involved water fractionation and fractional crystallization. These calculations indicate that during the initial exhumation stages water saturated mineral assemblages can be attained without external water supply.

Modelling of rock densities along the exhumational P-T path of HP rocks in the Sesia Zone indicate that the density contrast of the exhuming Sesia rock body with the surrounding mantle rocks increased between 1.5 and 1.0 GPa. This is due to the replacement of omphacite by sodic amphibole and albitic feldspar in metapelitic and metagranitoid rocks. The density contrast in this depth interval is sufficient to drive buoyant rise of the subducted rock body to the base of the crust of the upper plate provided that the rock body is of the order of several kilometres thick and that the surrounding rocks are weakened. Weakening is likely to occur either due to hydration of silicate minerals in the rock matrix (hydrolytic weakening), or to syntectonic grain size reduction, leading to deformation by viscous granular flow mechanisms. Our models show that once an exhuming rock body reaches the lower continental crust, buoyancy-driven exhumation slows or stops, and the exhumed rocks heats up. In the absence of continued exhumation, this can lead to thermal overprinting of the HP assemblages. In the case of the Sesia Zone, however, Late Cretaceous transpressional exhumation was sufficiently rapid to avoid such an overprint. Continued exhumation involving

extensional shearing brought the HP rocks of the Sesia Zone near to the surface by Early- to Mid Tertiary time.

Our results underscore the importance of deriving detailed P-T paths for exhumed HP assemblages as a basis for realistic thermo-mechanical modelling. Such assemblages provide us with the only information about conditions during the initial stages of exhumation in subduction zones. The modelling of elemental disequilibrium features along P-T paths allow us to quantify changes in volatile content and density associated with retrograde mineral reactions. These in turn constrain upward heat advection during exhumation and thus influence the strength of rocks in the upper plate of the subducting slab. .

5.7 ACKNOWLEDGEMENTS

We thank Claudio Rosenberg, Roland Oberhänsli and Patrick O'Brien for many interesting discussions on high pressure metamorphism and Alpine geology. Lutz Hecht is thanked for providing access to the electron microprobe facility of the Humboldt University, Berlin. The project was funded for two and a half years by the German Science Foundation grant Ha 2403/5. The first and third authors were each supported by a post-graduate studentship from the Freie Universität, Berlin.